
CHALMERS
UNIVERSITY OF TECHNOLOGY

# Charge Localization in Acene Crystals from Ab Initio Electronic Structure



Citation for the original published paper (version of record):
Ambrosio, F., Wiktor, J., Landi, A. et al (2023). Charge Localization in Acene Crystals from Ab Initio Electronic Structure. Journal of Physical Chemistry Letters: 3343-3351.
http://dx.doi.org/10.1021/acs.jpclett.3c00191

THE JOURNAL OF PHYSICAL CHEMISTRY LETTERS
A JOURNAL OF THE AMERICAN CHEMICAL SOCIETY

pubs.acs.org/JPCL

Letter

# Charge Localization in Acene Crystals from *Ab Initio* Electronic Structure

Francesco Ambrosio,* Julia Wiktor,* Alessandro Landi, and Andrea Peluso

Cite This: *J. Phys. Chem. Lett.* 2023, 14, 3343−3351

Read Online

ACCESS | Metrics & More | Article Recommendations | Supporting Information

**ABSTRACT:** The performance of Koopmans-compliant hybrid functionals in reproducing the electronic structure of organic crystals is tested for a series of acene crystals. The calculated band gaps are found to be consistent with those achieved with the *GW* method at a fraction of the computational cost and in excellent accord with the experimental results at room temperature, when including the thermal renormalization. The energetics of excess holes and electrons reveals a struggle between polaronic localization and band-like delocalization. The consequences of these results on the transport properties of acene crystals are discussed.

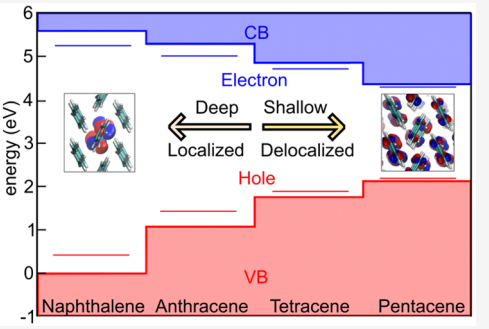




The pioneering studies of the last century on the optoelectronic properties of organic semiconductors based on $\pi$-conjugated systems[1−4] have paved the way for organics electronics.[5−7] These materials have come under the spotlight of the scientific community for their favorable properties, in particular a good flexibility,[8−11] making them attractive for a wide range of applications, including light-emitting diodes, thin-film transistors, and photovoltaics.[12−18] In this context, the manifold routes of organic synthesis allow for a vast chemical and structural versatility of organic semiconductors. This should translate, in principle, into an immense variety of electronic properties to be tuned for the desired application.[19] In fact, large sets of data, collected in the last decades, are available through online databases.[20,21] However, a clear-cut structure−property correlation is still missing, thus hindering the development of organic semiconductors with optimal features. In particular, achieving a satisfactory charge carrier mobility via rational materials design is key for the technological implementation of organic semiconductors as light-absorbers or charge transport layers in third-generation photovoltaics.[22−26]

The charge transport mechanism in organic semiconductors is still under debate,[22,27,28] since, as noted many times in the past, several theoretical methods have been able to predict results in good agreement with the experimental charge mobility,[23,29−33] despite relying on different physical assumptions, ranging from hopping to band-like transport. However, it has been argued that both the hopping and the band-like mechanism may be inadequate for treating charge transport in organic semiconductors.[22,34−40] Indeed, a genuine band-like mechanism is ruled out by the short mean free path observed in organic field-effect transistors,[27] while hopping, usually used in conjunction with rate constants obtained by Marcus theory, predicts a thermally activated mechanism not fully consistent with experimental observations.[41] That point of view has been questioned several times; indeed, the above observation is closely related to the use of classical theory of electron transfer. It has been demonstrated that the inclusion of quantum effects, nowadays extended to the whole bath provided by the intramolecular modes of redox units,[42] allows obtaining a dependence of the mobilities on the temperature in fairly good agreement with the experimental data.[30,43−45] Alternative models have been proposed, among which the transient localization theory is gaining an increasing popularity. This model is based on the idea that the unavoidable disorder in real crystals leads to a "transient localization" which would severely slow down carrier mobility. Nevertheless, time fluctuations of crystal disorder may still activate charge diffusion.[27,46]

In this context, reliable and affordable computational tools to determine the electronic properties of organic semiconductors can be game-changers, since the precise description of charge localization is paramount to define the proper charge transport mechanism.[22,27,30,32] Simplified computational schemes, which avoid a full atomistic description of organic crystals by performing calculations on single molecules embedded in an electrostatic cavity,[47] even if potentially useful for fast screening, cannot be employed to quantitatively

**Received:** January 20, 2023
**Accepted:** March 10, 2023
**Published:** March 30, 2023

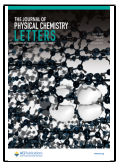





https://doi.org/10.1021/acs.jpclett.3c00191
*J. Phys. Chem. Lett.* 2023, 14, 3343−3351

describe other physical observables.[48] Therefore, solid-state *ab initio* calculations remain the most obvious choice to assess the electronic properties of organic semiconductors. However, on one side, the use of highly accurate methods based on many-body perturbation theory (e.g., the *GW* method[49−52]), although possibly being appropriate for a benchmark on a few model systems,[53−56] might be unaffordable for screening a plethora of materials. On the other side, density functional theory (DFT), the workhorse of computational materials science, fails in delivering quantitatively valid results,[57] in terms of band gaps and charge localization/polaron binding energies, a consequence of the self-interaction error.[58,59] While hybrid DFT methods[60−63] generally lead to improved results, the accuracy of the calculated electronic structure is still partially undermined by self-interaction,[64] as the amount of incorporated Fock exchange $\alpha$ is not satisfactorily defined. Since the band edges change linearly with $\alpha$, while the position of the energy levels associated with localized electronic states is essentially stable, if referred to the average electrostatic potential of the system,[65] errors in the opposite direction are possible, i.e., excessive localization and overestimation of polaron binding energies.

The recent idea of fixing the parameters of the density functional by imposing properties of the exact functional have ignited the development of nonempirical hybrid functionals.[66−72] In exact DFT, the energy level of a single-particle state is independent from electron occupation (generalized Koopmans' condition), thus ensuring the piecewise linearity of the functional upon fractional electron occupation.[73−75] The definition of the embodied $\alpha$ via fulfillment of the Koopmans' condition has given rise to the so-called Koopmans-compliant hybrid functionals, which were found to accurately reproduce the electronic properties (e.g., band gap, band edges, polaron binding energies) of both inorganic semiconductors and liquids at only a tiny fraction of the huge computational cost associated with the most advanced *GW* methods.[70,71,76−80] Therefore, this class of hybrid functionals might represent the much-needed computational tool to explore the boundless chemical and structural *mare magnum* of organic semiconductors, provided that their accuracy is adequately tested and benchmarked.

To this end, acene crystals are convenient model objects, being the archetypal organic molecular crystals and thus subject to a large number of studies.[13] In acene crystals, the building blocks, i.e., linear polycyclic aromatic hydrocarbons, are usually arranged in a herringbone structure (cf. Figure 1), with stabilization of the condensed phase provided by weak van der Waals interactions between molecules. A remarkably high degree of purity can be achieved for these crystals, which allows for in-depth experimental characterization of their intrinsic electronic properties.[81]

In this study, we report on the performance of Koopmans-compliant functionals for the calculation of the electronic structure of the most common acene crystals, namely, naphthalene, anthracene, tetracene, and pentacene (cf. Figure 1). For each material, we consider the simplest hybrid-DFT scheme, based on the PBE0[60,61] family of functionals, which was found to be provide results in line with those attained via Coulomb attenuated methods.[71,78,79] We employ the probe method[71,78,79] to determine the fraction of Fock exchange fulfilling the generalized Koopmans' condition. To assess the performance of the Koopmans-compliant hybrid functionals, we benchmark them against results obtained using the *GW*

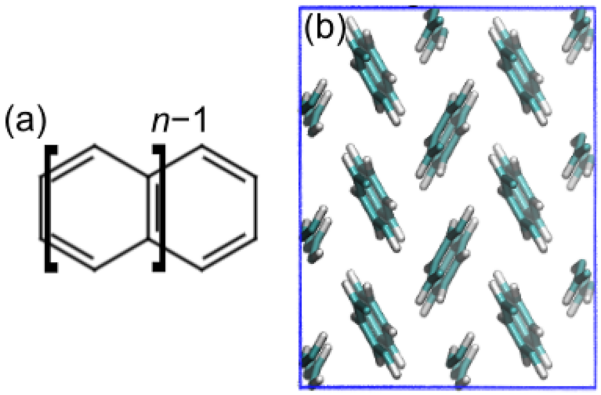


**Figure 1.** (a) General formula of linear acenes and (b) structural representation of the typical herringbone structure in which acene molecules crystallize, as observed from the 2 × 3 × 2 supercell employed for solid naphthalene. The *b* axis lies vertically.

approximation within the many-body perturbation theory. We perform one-shot *GW* calculations on top of energies and wave functions calculated within the Koopmans-compliant hybrid functionals. We include vertex corrections in the form of the bootstrap exchange−correlation kernel.[52,82] This results in the so-called $G_0\tilde{W}_0$@PBE0($\alpha_K$) scheme, which is expected to give accuracy close to that of the fully self-consistent *QSGW* method.[52,83] We compare the results calculated at the hybrid and $G_0\tilde{W}_0$@PBE0($\alpha_K$) levels of theory, and we find that both methods produce fundamental band gaps in very good accord with the experimental estimate at room temperature, provided that gap renormalization induced by thermal motion is properly included. We adopt the Koopmans-compliant functional to investigate charge localization in acene crystals, and from the calculated values of reorganization energies, we observe a struggle between polaronic localization and band-like delocalization, with the former being favored in naphthalene and anthracene and the latter more stable in tetracene and pentacene. Finally, we discuss how the present results can be related with charge transport properties observed for acene crystals.

We adopt the crystallographic structures obtained at room temperature,[84−87] which is necessary because acene crystals show both a sizable gap increase upon thermal lattice expansion and renormalization due to room-temperature disorder (e.g., refs 53 and 56). Space group, lattice parameters, and angles are reported in Table S1. To estimate the fraction of Fock exchange to be incorporated for the fulfillment of the generalized Koopmans' condition, $\alpha_K$, we construct 2 × 3 × 2 supercells containing up to 864 atoms (cf. Figure 1 for naphthalene and the Supporting Information). Then, we insert a single hydrogen atom, thus introducing a localized state in the band gap of the organic semiconductor, e.g., crystalline anthracene in Figure 2. Then, we calculate the single-particle energy level for both the occupied (neutral supercell, $H^0$) and unoccupied (positively charged, $H^+$) states at the hybrid-DFT level, considering three different values of $\alpha$. To alleviate the sizable computational cost associated with hybrid DFT for large supercells, we perform these calculations with the auxiliary density matrix method (ADMM) as implemented in the CP2K suite of programs (cf. the Supporting Information for computational details).[88−91] The intersection between the linear evolution of the energy levels for occupied and empty states[71] corresponds to $\alpha_K$ (cf. Figure 2). For comparison, we


https://doi.org/10.1021/acs.jpclett.3c00191
J. Phys. Chem. Lett. 2023, 14, 3343−3351

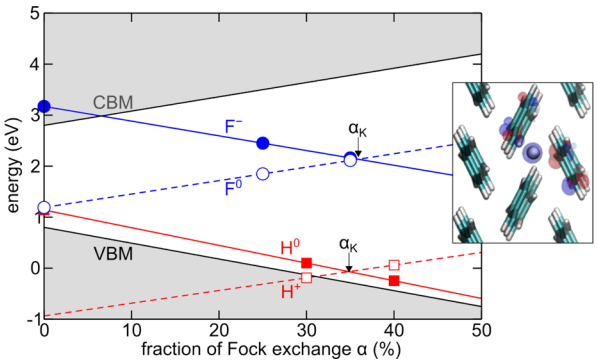


**Figure 2.** Occupied (full circles) and unoccupied (empty circles) single-particle energy levels of the interstitial hydrogen (red) and fluorine (blue) as a function of the fraction of Fock exchange $\alpha$ used in the PBE0 functional for solid anthracene. The $\alpha$-dependent evolution of the valence band maximum (VBM) and the conduction band minimum (CBM) are also reported (solid black lines). Energies are referred to the average electrostatic potential. The intersection points, corresponding to $\alpha_K$, are highlighted. Inset: Licorice representation of the hydrogen probe (gray, enlarged) inserted in a periodic supercell of crystalline anthracene along with the isodensity representation of the corresponding highest occupied molecular orbital.

have repeated the procedure substituting H with F: the convergence of the $-1/0$ energy levels illustrated in Figure 2 evidences negligible differences in the determination of $\alpha_K$, confirming the robustness of the employed methodology. Calculated values of $\alpha_K$ (cf. Table 2) are found in a minimal range, from 0.37 (naphthalene) to 0.33 (pentacene), a result which can be interpreted in terms of the similar dielectric response of these materials.[92−94]

Inclusion of disorder and atomic vibrations is crucial to achieve a meaningful comparison with measurements performed at room temperature. Therefore, we evaluate the band gap renormalization, which is known to be relevant for small-molecule acene crystals.[56,95] To this end, we perform Born−Oppenheimer molecular dynamics (MD) simulations at 300 K, in line with previous studies (cf. the Supporting Information for details),[96,97] employing the rVV10 functional[98,99] that self-consistently includes nonlocal electron correlation, which is required to accurately describe the structural features of acene crystals.[100−103] From cell optimizations, we have verified that this functional produces lattice parameters in excellent agreement with those of the available low-temperature crystallographic data (cf. the Supporting Information), thus ensuring that the *NVT*-MD electronic structure is not affected by unphysical dynamics.

The thermal band gap renormalization $\Delta E_g(T)$ is calculated at the PBE0($\alpha_K$) level from 100 structural configurations equally spaced in time. In particular, we consider

$$\Delta E_g(T) = \Delta E_V(T) + \Delta E_C(T) \quad (1)$$

where $\Delta E_V(T)$ and $\Delta E_C(T)$ are the individual contributions from the valence and conduction band edge, respectively, which are defined as

$$\Delta E_V(T) = E_V(T) - E_V(0) \quad (2)$$

and

$$\Delta E_C(T) = E_C(0) - E_C(T) \quad (3)$$

where $E_V(T)$ and $E_C(T)$ are the valence and conduction band edges at room temperature, while $E_V(0)$ and $E_C(0)$ are those calculated on the ordered crystallographic structure. We extract these quantities through linear extrapolations of the wings of the electronic density of states (DOS) near the band edges in order to eliminate the effect of the band tail[83,104] (cf. the Supporting Information).

Calculated values of $\Delta E_g(T)$ collected in Table 1 show that the temperature-dependent renormalization is more pronounced for smaller acenes, namely, naphthalene and anthracene, a feature that has been recently explained in terms of a stronger coupling with the low-frequency phonons for these materials.[95] The present results are consistent with those reported in the literature and achieved with electron−phonon self-energy,[56] tight-binding models,[46] and MD simulations on similar supercells.[95]

**Table 1. Calculated Absolute Values of the Thermal Renormalization of the Valence and Conduction Band Edges, $\Delta E_V(T)$ and $\Delta E_C(T)$, Respectively, and of the Band Gap $\Delta E_g(T)$, as Achieved from DFT-Based MD Simulations and Classical Molecular Mechanics (in parentheses)**

| material | $\Delta E_V(T)$ | $\Delta E_C(T)$ | $\Delta E_g(T)$ |
|---|---|---|---|
| naphthalene | 0.15 | 0.18 | 0.33 (0.30) |
| anthracene | 0.10 | 0.15 | 0.25 (0.21) |
| tetracene | 0.04 | 0.10 | 0.14 (0.11) |
| pentacene | 0.03 | 0.05 | 0.12 (0.08) |

Since DFT-based MD simulations are particularly expensive for the supercells that are necessary to adequately simulate acene crystals, we also consider, for comparison, the performance of classical molecular mechanics. To this end, we have constructed specific force fields for each acene (cf. the Supporting Information) and calculated $\Delta E_g(T)$ adopting the same procedure. The gap renormalization (in parentheses in Table 1) is in fair agreement with the DFT-MD value with differences up to 0.04 eV for anthracene, thus suggesting that such a cheaper procedure may be safely employed in high-throughput computational protocols.

We now focus on the fundamental band gaps of a set of acene crystals using the $G_0\tilde{W}_0$@PBE0($\alpha_K$) scheme at 0 K, $E_g(0)$. The results are presented in Table 2. We observe that the band gaps obtained at the $G_0\tilde{W}_0$@PBE0($\alpha_K$) level are in good agreement with those calculated using the Koopmans-compliant hybrid functional, indicating that our one-shot procedure is reasonably close to self-consistency. This also confirms the effectiveness of Koopmans-compliant hybrid functionals in this class of materials. Furthermore, we compare our results with previous *GW* calculations by Rangel et al.,[56] who employed both $G_0W_0$ and ev*GW* methods for a similar set of materials. The ev*GW* method partially achieves self-consistency with respect to the eigenvalues. Our calculated band gaps are generally smaller than those obtained using ev*GW* in ref 56, which is likely due to the inclusion of vertex corrections in our approach.

Next, we evaluate the accuracy of our computational scheme in predicting the band gaps of acenes at room temperature by comparing with experimental data. To do so, we define the theoretical room-temperature band gap as $E_g(T) = E_g(0) - \Delta E_g(T)$. As shown in Table 2, our predictions of band gaps at room temperature based on $G_0\tilde{W}_0$@PBE0($\alpha_K$) calculations are


https://doi.org/10.1021/acs.jpclett.3c00191
J. Phys. Chem. Lett. 2023, 14, 3343−3351

Table 2. Calculated Values of $\alpha_K$ (%), at 0 K and Room Temperature (RT), Band Gaps (in eV) at the PBE0($\alpha_K$) and $G_0\tilde{W}_0$@PBE0($\alpha_K$) Levels of Theory along with the Experimental Estimates[a]

| material | $\alpha_K$ | PBE0($\alpha_K$) 0 K | $G_0\tilde{W}_0$@PBE0($\alpha_K$) 0 K | PBE0($\alpha_K$) RT | $G_0\tilde{W}_0$@PBE0($\alpha_K$) RT | exptl |
|---|---|---|---|---|---|---|
| naphthalene | 37 | 5.56 (5.58) | 5.68 | 5.23 (5.25) | 5.35 | 5.0−5.4[105,106] |
| anthracene | 35 | 4.12 (4.20) | 4.26 | 3.86 (3.95) | 4.01 | 3.9−4.0[105,107] |
| tetracene | 34 | 2.86 (3.04) | 2.97 | 2.76 (2.90) | 2.83 | 2.8−3.1[107,108] |
| pentacene | 33 | 2.26 (2.22) | 2.25 | 2.14 (2.10) | 2.13 | 2.1−2.2[109,110] |

[a]In parentheses, the values calculated with the ADMM/supercell approach are reported. $\Delta E_g(T)$ as calculated from DFT-MD molecular dynamics is included in the RT values.

in good agreement with the experimental values for all materials. For comparison, we also present the band gaps calculated at the PBE0($\alpha_K$) level using the ADMM/supercell computational scheme employed to determine $\alpha_K$. The consistent agreement between our predictions and the experimental data indicates that this method can be reliably applied to study the electronic structure of organic materials.

We now investigate charge localization in the acene family. To this end, we perform structural relaxation of the supercells with an extra hole and an electron. This allows us to define the reorganization energy of the acene crystal

$$\lambda^q(\text{crys}) = E^q_{\text{vert}}(\text{crys}) - E^q_{\text{opt}}(\text{crys}) \quad (4)$$

as the difference between the total energy of the relaxed charged supercell [$E^q_{\text{opt}}$(crys)] and that with the nuclei fixed to the equilibrium positions of the neutral system [$E^q_{\text{vert}}$(crys)], the latter representing the energy associated with charge delocalization. We note that the positive value of $\lambda$ indicates that localization is favorable, while the negative value suggests that the localized state is not stable. Furthermore, to disentangle the different effects contributing to the stabilization of the excess charges, we adopt the following computational protocol: First, for each acene, we isolate a single molecule from the supercell, we place it in vacuum, and we perform a structural relaxation with an excess charge $q$. This allows localizing $q$ on a single molecule and defining the molecular reorganization energy

$$\lambda^q(\text{mol}) = E^q_{\text{vert}}(\text{mol}) - E^q_{\text{opt}}(\text{mol}) \quad (5)$$

as the total-energy difference between the isolated molecule upon vertical injection of the charge [$E^q_{\text{vert}}$(mol)] and the optimized molecule [$E^q_{\text{opt}}$(mol)]. Then, the charged molecule is reintroduced in the supercell, thus replacing that previously extracted. This model allows us to calculate the energy gain associated with localization of the charge on a single molecule $\lambda^q$(loc) with respect to delocalization on the band edge:

$$\lambda^q(\text{loc}) = E^q_{\text{vert}}(\text{crys}) - E^q_{\text{loc}}(\text{crys}) \quad (6)$$

where $E^q_{\text{loc}}$(crys) is the total energy of the supercell with $q$ localized on a single molecule. Since we have verified that full relaxation of the charged supercells starting either from the structure of the neutral crystal or from the localized model produces the same final structure, the effect of the environment $\lambda^q$(env) is evaluated as

$$\lambda^q(\text{env}) = E^q_{\text{loc}}(\text{crys}) - E^q_{\text{opt}}(\text{crys}) \quad (7)$$

from which it follows that

$$\lambda^q(\text{crys}) = \lambda^q(\text{loc}) + \lambda^q(\text{env}) \quad (8)$$

For a visual aid, the different reorganization energies are summarized in Scheme 1.

Scheme 1. Schematic Representation of the Calculated Reorganization Energies, as Defined in the Main Text[a]

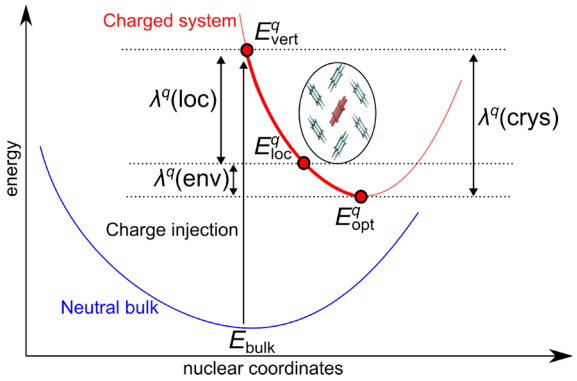


[a]The scheme refers to the cases for which charge localization on a single molecule is more stable than the system upon vertical charge injection.

Reorganization energies associated with hole and electron injection, $\lambda^+$ and $\lambda^-$, respectively, are collected in Table 3. First, we note that the present results on the single molecules are in line with previous calculations and experiments, with the observed trends of decreasing $\lambda^q$(mol) for longer acenes and slightly larger values of reorganization for electrons nicely reproduced.[111−113]

Table 3. Calculated Values of Reorganization Energies (cf. main text for details) for the Acene Crystals Considered in This Study[a]

| | hole localization | | | |
|---|---|---|---|---|
| | $\lambda^+$(mol) | $\lambda^+$(loc) | $\lambda^+$(env) | $\lambda^+$(crys) |
| naphthalene | 0.11 | 0.14 | 0.08 | 0.22 |
| anthracene | 0.09 | 0.14 | 0.06 | 0.20 |
| tetracene | 0.08 | −0.04 | 0.09[b] | 0.05 |
| pentacene | 0.06 | −0.08 | 0.10[b] | 0.02 |
| | electron localization | | | |
| | $\lambda^-$(mol) | $\lambda^-$(loc) | $\lambda^-$(env) | $\lambda^-$(crys) |
| naphthalene | 0.15 | 0.15 | 0.12 | 0.27 |
| anthracene | 0.12 | 0.10 | 0.08 | 0.18 |
| tetracene | 0.10 | −0.05 | 0.11[b] | 0.06 |
| pentacene | 0.08 | −0.07 | 0.08[b] | 0.01 |

[a]All values are given in eV. [b]Values do not refer to an additional stabilization of localized charges given by the environment as in these cases charge localization is unfavorable.



https://doi.org/10.1021/acs.jpclett.3c00191
J. Phys. Chem. Lett. 2023, 14, 3343−3351

Data calculated on supercells allow distinguishing two different behaviors upon charge injection, with minor differences between holes and electrons. In fact, for naphthalene and anthracene crystals, values of $\lambda^q$(loc) above 0.1 eV indicate that polaronic localization of the charge on a single molecule is favorable with respect to delocalization on the band edge states. Furthermore, the response of the surrounding molecules denoted by $\lambda^q$(env) enhances the stabilization of the charge. The latter remains largely confined on one molecule, whose nuclei positions almost do not change during relaxation, thus indicating an exiguous charge transfer toward surrounding molecules (cf. Figure 3), in line with a very recent study

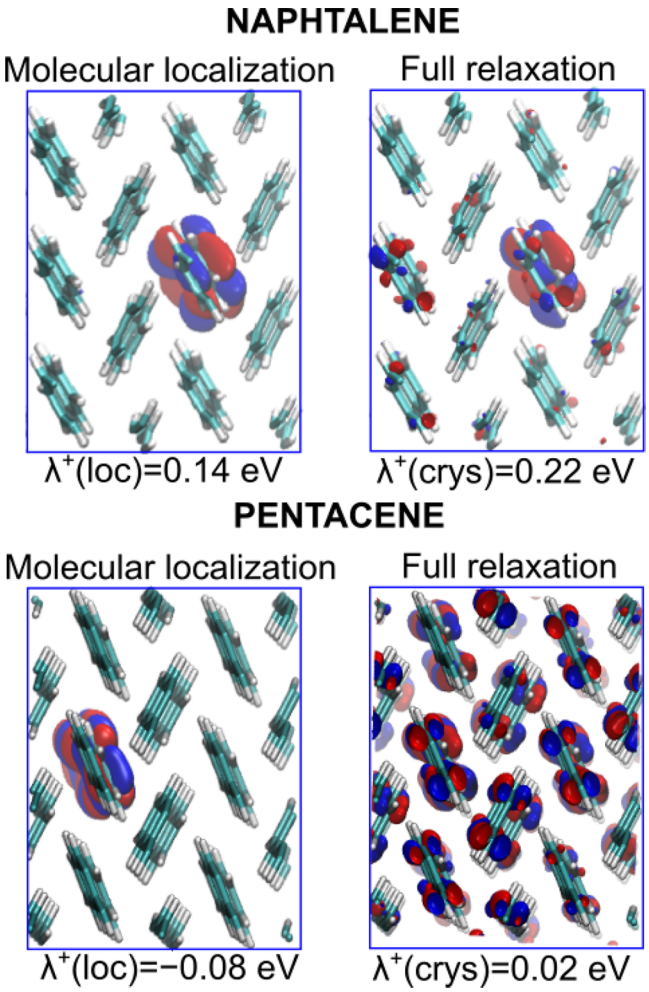


**Figure 3.** Isodensity representation of the lowest unoccupied molecular orbital (LUMO) for positively charged supercells of crystalline naphthalene (top) and pentacene (bottom). Left panels depict charge localization on a single molecule (cf. main text), while right panels illustrate the LUMO of the fully relaxed charged supercell.

showing that polaronic localization in naphthalene arises from intramolecular phonons.[114] We further note that the calculated $\lambda^q$(env) values are somewhat larger than those from previous study in which this contribution however was evaluated from classical molecular mechanics.[115] Nevertheless, the trends are qualitatively consistent.

In stark contrast, the negative values of $\lambda^q$(loc) for tetracene and pentacene imply that charge localization is slightly unfavorable in these cases; that is, the localized states are essentially resonant with band edges. In fact, upon full relaxation of the charged system, both holes and electrons are found to be substantially delocalized, as evidenced by the extremely small values of $\lambda^q$(crys) and by the analysis of the pertinent molecular orbitals (cf. pentacene in Figure 3). This is accompanied mainly by relaxation of the molecule bearing the charge which restores its structural configuration in the neutral crystal.

Finally, we calculate the charge transition levels of the polaronic defects with respect to the band edges of each acene, using a grand-canonical formulation of defects in crystalline materials.[116,117] Within this theory, the formation energy of a defect $X$ in a charge state $q$ is

$$E_f^q[X] = E^q[X] - E[\text{bulk}] + q(\mu + \epsilon_V) \tag{9}$$

where $E$[bulk] and $E^q[X]$ are the total energies of the pristine bulk of the supercell bearing the defect, $\mu$ is the electron chemical potential, and $\epsilon_V$ is the valence band edge of the semiconductor. The energy level corresponding to a transition from a charge state $q$ to $q'$ of a defect $X$ is defined as the Fermi level for which their formation energies are equal, $E_f^q[X] = E_f^{q'}[X]$:

$$\mu(q/q') = \frac{E^q[X] - E^{q'}[X]}{q' - q} - \epsilon_V \tag{10}$$

For polarons, $E^q[X] = E^+$[loc], $E^-$[loc] for localized hole and electron respectively, while $E_f^{q'}[X] = E$[bulk].[77,118] Therefore

$$\mu(+1/0) = -E^+[\text{loc}] + E[\text{bulk}] - \epsilon_V \tag{11}$$

and

$$\mu(-1/0) = E^-[\text{loc}] - E[\text{bulk}] - \epsilon_V \tag{12}$$

In Figure 4, the polaronic charge transition levels, as calculated from eqs 11 and 12, are reported for each acene

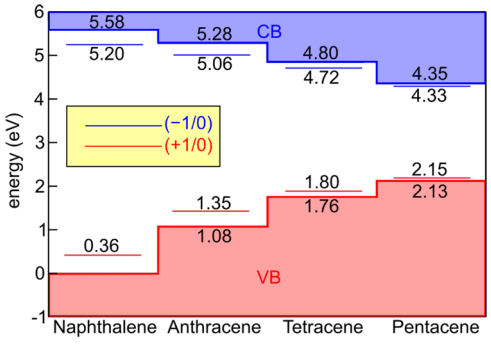


**Figure 4.** Calculated polaronic charge transition levels (cf. eqs 11 and 12, main text) for the considered acene crystals. Energies are referred to the valence band of naphthalene and are aligned via the valence band spectra of ref 119. For consistency, 0 K band gaps from Table 2 are considered.

crystal. The energy levels of different acenes are aligned via the measured valence band spectra of ref 119, and the hybrid-DFT 0 K values of the band gaps from Table 2 are considered. In line with the observed values of $\lambda$, calculated energy levels for localized holes (electrons) in naphthalene and anthracene are clearly above (below) the valence (conduction) band edge. At variance with this, tetracene and pentacene feature shallow energy levels, essentially resonant with the respective band edges. We note that, while thermal renormalization reduces the



https://doi.org/10.1021/acs.jpclett.3c00191
J. Phys. Chem. Lett. 2023, 14, 3343−3351

band gap, thus possibly affecting the energy diagram, at the same time, room-temperature disorder is known to stabilize localized charges in both organic and inorganic semiconductors[77,120,121] and will deserve further consideration.

The struggle between localization and delocalization denoted by the calculated values of $\lambda$ and of the charge transition levels can help rationalizing the transport properties of these materials, which have long puzzled the research community as they typically fall in a transport regime at the boundaries between the limit cases describable with either band transport or charge hopping.[29,120,122] In this context, our computational analysis suggests that a small or midsized polaron hopping model might be justified for naphthalene and anthracene. However, such a model cannot hold for tetracene and pentacene as our analysis shows larger delocalization of charge carriers. Therefore, band-like/large polaron models are preferable, in line with the view recently proposed on the basis of nonadiabatic molecular dynamics.[25,32]

In conclusion, we have shown that Koopmans-compliant hybrid functionals represent a reliable and efficient tool to rapidly evaluate the band gap of acene crystals, with results consistent with those achieved with the *GW* method and in excellent agreement with experimental results, when thermal renormalization of the gap is properly accounted for. The employed methodology, devoid of the self-interaction error, allowed for an in-depth analysis of charge localization in different acenes, which highlighted a struggle between localization and delocalization of the charge carriers: for shorter acenes, namely naphthalene and anthracene, polaronic localization appears to be energetically favored; at variance with this, holes and electrons in tetracene and pentacene are endowed with a larger delocalization. Overall, the present results may aid the rationalization of the charge transport properties of acene crystals and the use of the presented methodology can be extended to other organic crystals.

## ■ ASSOCIATED CONTENT

### Supporting Information

The Supporting Information is available free of charge at https://pubs.acs.org/doi/10.1021/acs.jpclett.3c00191.

Computational details, benchmark of the employed rVV10 functional on low-temperature crystallographic structures, linear extrapolation of the electronic density of states for the calculation of the band gap, and additional references (PDF)

## ■ AUTHOR INFORMATION


### Corresponding Authors

**Francesco Ambrosio** − *Dipartimento di Chimica e Biologia Adolfo Zambelli, Università di Salerno, I-84084 Fisciano, SA, Italy; Dipartimento di Scienze, Università degli Studi della Basilicata, 10-85100 Potenza, Italy;* orcid.org/0000-0002-6388-9586; Email: fambrosio@unisa.it

**Julia Wiktor** − *Department of Physics, Chalmers University of Technology, SE-412 96 Gothenburg, Sweden;* orcid.org/0000-0003-3395-1104; Email: julia.wiktor@chalmers.se

### Authors

**Alessandro Landi** − *Dipartimento di Chimica e Biologia Adolfo Zambelli, Università di Salerno, I-84084 Fisciano, SA, Italy;* orcid.org/0000-0003-3627-5535

**Andrea Peluso** − *Dipartimento di Chimica e Biologia Adolfo Zambelli, Università di Salerno, I-84084 Fisciano, SA, Italy;* orcid.org/0000-0002-6140-9825

Complete contact information is available at: https://pubs.acs.org/10.1021/acs.jpclett.3c00191


### Notes

The authors declare no competing financial interest.

## ■ ACKNOWLEDGMENTS

We acknowledge financial support from the Università di Salerno, grants: FARB 2020 and FARB 2021. F.A. acknowledges REACT-EU DM 1062/2021 for funding and the CINECA project AID-Loc for computational resources. J.W. acknowledges funding from "Genie", "Area of Advance - Materials Science" at Chalmers University of Technology, and the Swedish Research Council (2019-03993). The computations were partly performed on resources provided by the Swedish National Infrastructure for Computing (SNIC) at NSC, C3SE, and PDC.

## ■ REFERENCES


(1) Chiang, C. K.; Fincher, C. R.; Park, Y. W.; Heeger, A. J.; Shirakawa, H.; Louis, E. J.; Gau, S. C.; MacDiarmid, A. G. Electrical Conductivity in Doped Polyacetylene. *Phys. Rev. Lett.* **1977**, *39*, 1098−1101.

(2) Ebisawa, F.; Kurokawa, T.; Nara, S. Electrical Properties of Polyacetylene/Polysiloxane Interface. *J. Appl. Phys.* **1983**, *54*, 3255−3259.

(3) Tang, C. W.; VanSlyke, S. A. Organic Electroluminescent Diodes. *Appl. Phys. Lett.* **1987**, *51*, 913−915.

(4) Burroughes, J. H.; Bradley, D. D.; Brown, A.; Marks, R.; Mackay, K.; Friend, R. H.; Burns, P. L.; Holmes, A. B. Light-Emitting Diodes Based on Conjugated Polymers. *Nature* **1990**, *347*, 539−541.

(5) Muccini, M. A. Bright Future for Organic Field-Effect Transistors. *Nat. Mater.* **2006**, *5*, 605−613.

(6) Pope, M.; Swenberg, C. E.; et al. *Electronic Processes in Organic Crystals and Polymers*; Oxford University Press on Demand, 1999; Vol. *56*.

(7) Silins, E.; Capek, V. *Organic Molecular Crystals: Interaction, Localization, and Transport Phenomena*; American Inst. of Physics, 1994.

(8) Wu, Y.; Chew, A. R.; Rojas, G. A.; Sini, G.; Haugstad, G.; Belianinov, A.; Kalinin, S. V.; Li, H.; Risko, C.; Brédas, J.-L.; Salleo, A.; Frisbie, C. D. Strain Effects on the Work Function of an Organic Semiconductor. *Nat. Commun.* **2016**, *7*, 10270.

(9) Zhang, Z.; Yu, G.; Garcia-Barriocanal, J.; Xie, Z.; Frisbie, C. D. Strain-Work Function Relationship in Single-Crystal Tetracene. *ACS Appl. Mater. & Interfaces* **2020**, *12*, 40607−40612.

(10) Landi, A.; Peluso, A.; Troisi, A. Quantitative Prediction of the Electro-Mechanical Response in Organic Crystals. *Adv. Mater.* **2021**, *33*, 2008049.

(11) Root, S. E.; Savagatrup, S.; Printz, A. D.; Rodriquez, D.; Lipomi, D. J. Mechanical Properties of Organic Semiconductors for Stretchable, Highly Flexible, and Mechanically Robust Electronics. *Chem. Rev.* **2017**, *117*, 6467−6499.

(12) Nelson, J. Solar Cells by Self-Assembly? *Science* **2001**, *293*, 1059−1060.

(13) Wang, C.; Dong, H.; Hu, W.; Liu, Y.; Zhu, D. Semiconducting $\pi$-conjugated Systems in Field-Effect Transistors: A Material Odyssey of Organic Electronics. *Chem. Rev.* **2012**, *112*, 2208−2267.

(14) Xie, W.; McGarry, K. A.; Liu, F.; Wu, Y.; Ruden, P. P.; Douglas, C. J.; Frisbie, C. D. High-Mobility Transistors Based on Single Crystals of Isotopically Substituted Rubrene-d28. *J. Phys. Chem. C* **2013**, *117*, 11522−11529.

(15) Ren, X.; Bruzek, M. J.; Hanifi, D. A.; Schulzetenberg, A.; Wu, Y.; Kim, C.-H.; Zhang, Z.; Johns, J. E.; Salleo, A.; Fratini, S.; Troisi, A.; Douglas, C. J.; Frisbie, C. D. Negative Isotope Effect on Field-Effect Hole Transport in Fully Substituted $^{13}$C-Rubrene. *Adv. Electron. Mater.* **2017**, *3*, 1700018.
(16) Zhang, X.; Dong, H.; Hu, W. Organic Semiconductor Single Crystals for Electronics and Photonics. *Adv. Mater.* **2018**, *30*, 1801048.
(17) Wang, Y.; Sun, L.; Wang, C.; Yang, F.; Ren, X.; Zhang, X.; Dong, H.; Hu, W. Organic Crystalline Materials in Flexible Electronics. *Chem. Soc. Rev.* **2019**, *48*, 1492−1530.
(18) Wang, Y.; Lee, J.; Hou, X.; Labanti, C.; Yan, J.; Mazzolini, E.; Parhar, A.; Nelson, J.; Kim, J.-S.; Li, Z. Recent Progress and Challenges toward Highly Stable Nonfullerene Acceptor-Based Organic Solar Cells. *Adv. Energy Mater.* **2021**, *11*, 2003002.
(19) Wang, C.; Dong, H.; Jiang, L.; Hu, W. Organic Semiconductor Crystals. *Chem. Soc. Rev.* **2018**, *47*, 422−500.
(20) Kunkel, C.; Margraf, J. T.; Chen, K.; Oberhofer, H.; Reuter, K. Active Discovery of Organic Semiconductors. *Nat. commun.* **2021**, *12*, 2422.
(21) Pulido, A.; Chen, L.; Kaczorowski, T.; Holden, D.; Little, M. A.; Chong, S. Y.; Slater, B. J.; McMahon, D. P.; Bonillo, B.; Stackhouse, C. J.; et al. Functional Materials Discovery Using Energy−Structure−Function Maps. *Nature* **2017**, *543*, 657−664.
(22) Fratini, S.; Ciuchi, S.; Mayou, D.; De Laissardière, G. T.; Troisi, A. A Map of High-Mobility Molecular Semiconductors. *Nat. Mater.* **2017**, *16*, 998−1002.
(23) Fratini, S.; Nikolka, M.; Salleo, A.; Schweicher, G.; Sirringhaus, H. Charge transport in high-mobility conjugated polymers and molecular semiconductors. *Nat. Mater.* **2020**, *19*, 491−502.
(24) Nematiaram, T.; Padula, D.; Landi, A.; Troisi, A. On the Largest Possible Mobility of Molecular Semiconductors and How to Achieve it. *Adv. Funct. Mater.* **2020**, *30*, 2001906.
(25) Giannini, S.; Blumberger, J. Charge Transport in Organic Semiconductors: The Perspective from Nonadiabatic Molecular Dynamics. *Acc. Chem. Res.* **2022**, *55*, 819−830.
(26) Del Cueto, M.; Rawski-Furman, C.; Arago, J.; Orti, E.; Troisi, A. Data-Driven Analysis of Hole-Transporting Materials for Perovskite Solar Cells Performance. *J. Phys. Chem. C* **2022**, *126*, 13053−13061.
(27) Fratini, S.; Mayou, D.; Ciuchi, S. The Transient Localization Scenario for Charge Transport in Crystalline Organic Materials. *Adv. Funct. Mater.* **2016**, *26*, 2292−2315.
(28) Kirchartz, T.; Nelson, J. *Topics in Current Chemistry*; Springer: Berlin, 2013; pp 279−324.
(29) Nematiaram, T.; Troisi, A. Modeling Charge Transport in High-Mobility Molecular Semiconductors: Balancing Electronic Structure and Quantum Dynamics Methods with the Help of Experiments. *J. Chem. Phys.* **2020**, *152*, 190902.
(30) Landi, A. Charge Mobility Prediction in Organic Semiconductors: Comparison of Second-Order Cumulant Approximation and Transient Localization Theory. *J. Phys. Chem. C* **2019**, *123*, 18804−18812.
(31) Landi, A.; Borrelli, R.; Capobianco, A.; Velardo, A.; Peluso, A. Hole Hopping Rates in Organic Semiconductors: A Second-Order Cumulant Approach. *J. Chem. Theory Comput.* **2018**, *14*, 1594−1601.
(32) Giannini, S.; Carof, A.; Ellis, M.; Yang, H.; Ziogos, O. G.; Ghosh, S.; Blumberger, J. Quantum Localization and Delocalization of Charge Carriers in Organic Semiconducting Crystals. *Nat. Commun.* **2019**, *10*, 3843.
(33) Landi, A.; Troisi, A.; Peluso, A. Explaining Different Experimental Hole Mobilities: Influence of Polymorphism on Dynamic Disorder in Pentacene. *J. Mater. Chem. C* **2019**, *7*, 9665−9670.
(34) Troisi, A.; Orlandi, G. Charge-Transport Regime of Crystalline Organic Semiconductors: Diffusion Limited by Thermal Off-Diagonal Electronic Disorder. *Phys. Rev. Lett.* **2006**, *96*, 086601.
(35) Troisi, A. Prediction of the Absolute Charge Mobility of Molecular Semiconductors: the Case of Rubrene. *Adv. Mater.* **2007**, *19*, 2000−2004.
(36) Ortmann, F.; Bechstedt, F.; Hannewald, K. Charge Transport in Organic Crystals: Theory and Modelling. *Phys. Stat. Sol. (b)* **2011**, *248*, 511−525.
(37) Ren, J.; Vukmirović, N.; Wang, L.-W. Nonadiabatic Molecular Dynamics Simulation for Carrier Transport in a Pentathiophene Butyric Acid Monolayer. *Phys. Rev. B* **2013**, *87*, 205117.
(38) Heck, A.; Kranz, J. J.; Kubar, T.; Elstner, M. Multi-Scale Approach to Non-Adiabatic Charge Transport in High-Mobility Organic Semiconductors. *J. Chem. Theory Comput.* **2015**, *11*, 5068−5082.
(39) Landi, A.; Troisi, A. Rapid Evaluation of Dynamic Electronic Disorder in Molecular Semiconductors. *J. Phys. Chem. C* **2018**, *122*, 18336−18345.
(40) Xie, W.; Holub, D.; Kubar, T.; Elstner, M. Performance of Mixed Quantum-Classical Approaches on Modeling the Crossover from Hopping to Bandlike Charge Transport in Organic Semiconductors. *J. Chem. Theory Comput.* **2020**, *16*, 2071−2084.
(41) Cheng, Y. C.; Silbey, R. J.; da Silva Filho, D. A.; Calbert, J. P.; Cornil, J.; Brédas, J. L. Three-Dimensional Band Structure and Bandlike Mobility in Oligoacene Single Crystals: A Theoretical Investigation. *J. Chem. Phys.* **2003**, *118*, 3764−3774.
(42) Leo, A.; Peluso, A. Electron Transfer Rates in Polar and Non-Polar Environments: a Generalization of Marcus' Theory to Include an Effective Treatment of Tunneling Effects. *J. Phys. Chem. Lett.* **2022**, *13*, 9148−9155.
(43) Wang, L.; Nan, G.; Yang, X.; Peng, Q.; Li, Q.; Shuai, Z. Computational Methods for Design of Organic Materials with High Charge Mobility. *Chem. Soc. Rev.* **2010**, *39*, 423−434.
(44) Nan, G.; Yang, X.; Wang, L.; Shuai, Z.; Zhao, Y. Nuclear Tunneling Effects of Charge Transport in Rubrene, Tetracene, and Pentacene. *Phys. Rev. B* **2009**, *79*, 115203.
(45) Landi, A.; Borrelli, R.; Capobianco, A.; Velardo, A.; Peluso, A. Second-Order Cumulant Approach for the Evaluation of Anisotropic Hole Mobility in Organic Semiconductors. *J. Phys. Chem. C* **2018**, *122*, 25849−25857.
(46) Ciuchi, S.; Hatch, R. C.; Höchst, H.; Faber, C.; Blase, X.; Fratini, S. Molecular Fingerprints in the Electronic Properties of Crystalline Organic Semiconductors: From Experiment to Theory. *Phys. Rev. Lett.* **2012**, *108*, 256401.
(47) Krumland, J.; Gil, G.; Corni, S.; Cocchi, C. LayerPCM: An Implicit Scheme for Dielectric Screening from Layered Substrates. *J. Chem. Phys.* **2021**, *154*, 224114.
(48) Cocchi, C.; Guerrini, M.; Krumland, J.; Nguyen, N. T.; Valencia, A. M. Modeling the Electronic Structure of Organic Materials: A solid-State Physicist's Perspective. *arXiv* **2022**, 2208.09168.
(49) Hedin, L. New Method for Calculating the One-Particle Green's Function with Application to the Electron-Gas Problem. *Phys. Rev.* **1965**, *139*, A796−A823.
(50) van Schilfgaarde, M.; Kotani, T.; Faleev, S. Quasiparticle Self-Consistent *GW* Theory. *Phys. Rev. Lett.* **2006**, *96*, 226402.
(51) Shishkin, M.; Marsman, M.; Kresse, G. Accurate Quasiparticle Spectra from Self-Consistent GW Calculations with Vertex Corrections. *Phys. Rev. Lett.* **2007**, *99*, 246403.
(52) Chen, W.; Pasquarello, A. Accurate Band Gaps of Extended Systems via Efficient Vertex Corrections in *GW*. *Phys. Rev. B* **2015**, *92*, 041115.
(53) Brown-Altvater, F.; Antonius, G.; Rangel, T.; Giantomassi, M.; Draxl, C.; Gonze, X.; Louie, S. G.; Neaton, J. B. Band Gap Renormalization, Carrier Mobilities, and the Electron-Phonon Self-Energy in Crystalline Naphthalene. *Phys. Rev. B* **2020**, *101*, 165102.
(54) Sharifzadeh, S.; Biller, A.; Kronik, L.; Neaton, J. B. Quasiparticle and Optical Spectroscopy of the Organic Semiconductors Pentacene and PTCDA from First Principles. *Phys. Rev. B* **2012**, *85*, 125307.


https://doi.org/10.1021/acs.jpclett.3c00191
J. Phys. Chem. Lett. 2023, 14, 3343−3351

(55) Sharifzadeh, S.; Wong, C. Y.; Wu, H.; Cotts, B. L.; Kronik, L.; Ginsberg, N. S.; Neaton, J. B. Relating the Physical Structure and Optoelectronic Function of Crystalline TIPS-Pentacene. *Adv. Funct. Mater.* **2015**, *25*, 2038−2046.
(56) Rangel, T.; Berland, K.; Sharifzadeh, S.; Brown-Altvater, F.; Lee, K.; Hyldgaard, P.; Kronik, L.; Neaton, J. B. Structural and Excited-State Properties of Oligoacene Crystals from First Principles. *Phys. Rev. B* **2016**, *93*, 115206.
(57) Hummer, K.; Ambrosch-Draxl, C. Electronic Properties of Oligoacenes from First Principles. *Phys. Rev. B* **2005**, *72*, 205205.
(58) Perdew, J. P.; Zunger, A. Self-Interaction Correction to Density-Functional Approximations for Many-Electron Systems. *Phys. Rev. B* **1981**, *23*, 5048−5079.
(59) Zhang, Y.; Yang, W. A Challenge for Density Functionals: Self-Interaction Error Increases for Systems with a Noninteger Number of Electrons. *J. Chem. Phys.* **1998**, *109*, 2604−2608.
(60) Perdew, J. P.; Ernzerhof, M.; Burke, K. Rationale for Mixing Exact Exchange with Density Functional Approximations. *J. Chem. Phys.* **1996**, *105*, 9982−9985.
(61) Adamo, C.; Barone, V. Toward Reliable Density Functional Methods without Adjustable Parameters: The PBE0Model. *J. Chem. Phys.* **1999**, *110*, 6158−6170.
(62) Becke, A. D. A. New Mixing of Hartree−Fock and Local Density-Functional Theories. *J. Chem- Phys.* **1993**, *98*, 1372−1377.
(63) Heyd, J.; Scuseria, G. E.; Ernzerhof, M. Hybrid Functionals Based on a Screened Coulomb Potential. *J. Chem. Phys.* **2003**, *118*, 8207−8215.
(64) Atalla, V.; Zhang, I. Y.; Hofmann, O. T.; Ren, X.; Rinke, P.; Scheffler, M. Enforcing the Linear Behavior of the Total Energy with Hybrid Functionals: Implications for Charge Transfer, Interaction Energies, and the Random-Phase Approximation. *Phys. Rev. B* **2016**, *94*, 035140.
(65) Alkauskas, A.; Broqvist, P.; Pasquarello, A. Defect Levels through Hybrid Density Functionals: Insights and Applications. *Phys. Status Solidi B* **2011**, *248*, 775−789.
(66) Skone, J. H.; Govoni, M.; Galli, G. Self-Consistent Hybrid Functional for Condensed Systems. *Phys. Rev. B* **2014**, *89*, 195112.
(67) Skone, J. H.; Govoni, M.; Galli, G. Nonempirical Range-Separated Hybrid Functionals for Solids and Molecules. *Phys. Rev. B* **2016**, *93*, 235106.
(68) Gerosa, M.; Bottani, C.; Di Valentin, C.; Onida, G.; Pacchioni, G. Accuracy of Dielectric-Dependent Hybrid Functionals in the Prediction of Optoelectronic Properties of Metal Oxide Semiconductors: A Comprehensive Comparison with Many-Body *GW* and Experiments. *J. Phys.: Condens. Matter* **2018**, *30*, 044003.
(69) Zheng, H.; Govoni, M.; Galli, G. Dielectric-Dependent Hybrid Functionals for Heterogeneous Materials. *Phys. Rev. Materials* **2019**, *3*, 073803.
(70) Miceli, G.; Chen, W.; Reshetnyak, I.; Pasquarello, A. Nonempirical Hybrid Functionals for Band Gaps and Polaronic Distortions in Solids. *Phys. Rev. B* **2018**, *97*, 121112.
(71) Bischoff, T.; Reshetnyak, I.; Pasquarello, A. Adjustable Potential Probes for Band-Gap Predictions of Extended Systems through Nonempirical Hybrid Functionals. *Phys. Rev. B* **2019**, *99*, 201114.
(72) Deák, P.; Lorke, M.; Aradi, B.; Frauenheim, T. Optimized Hybrid Functionals for Defect Calculations in Semiconductors. *J. Appl. Phys.* **2019**, *126*, 130901.
(73) Perdew, J. P.; Parr, R. G.; Levy, M.; Balduz, J. L. Density-Functional Theory for Fractional Particle Number: Derivative Discontinuities of the Energy. *Phys. Rev. Lett.* **1982**, *49*, 1691−1694.
(74) Janak, J. F. Proof that $\partial E/\partial n_i = \epsilon$ in Density-Functional Theory. *Phys. Rev. B* **1978**, *18*, 7165−7168.
(75) Yang, W.; Zhang, Y.; Ayers, P. W. Degenerate Ground States and a Fractional Number of Electrons in Density and Reduced Density Matrix Functional Theory. *Phys. Rev. Lett.* **2000**, *84*, 5172−5175.
(76) Brawand, N. P.; Govoni, M.; Vörös, M.; Galli, G. Performance and Self-Consistency of the Generalized Dielectric Dependent Hybrid Functional. *J. Chem. Theory Comput.* **2017**, *13*, 3318−3325. PMID: 28537727.
(77) Ambrosio, F.; Wiktor, J.; De Angelis, F.; Pasquarello, A. Origin of Low Electron-Hole Recombination Rate in Metal Halide Perovskites. *Energy Environ. Sci.* **2018**, *11*, 101−105.
(78) Bischoff, T.; Wiktor, J.; Chen, W.; Pasquarello, A. Nonempirical Hybrid Functionals for Band Gaps of Inorganic Metal-Halide Perovskites. *Phys. Rev. Materials* **2019**, *3*, 123802.
(79) Bischoff, T.; Reshetnyak, I.; Pasquarello, A. Band gaps of Liquid Water and Hexagonal Ice through Advanced Electronic-Structure Calculations. *Phys. Rev. Research* **2021**, *3*, 023182.
(80) Ouhbi, H.; Ambrosio, F.; De Angelis, F.; Wiktor, J. Strong Electron Localization in Tin Halide Perovskites. *J. Phys. Chem. Lett.* **2021**, *12*, 5339−5343.
(81) Anthony, J. E. Functionalized Acenes and Heteroacenes for Organic Electronics. *Chem. Rev.* **2006**, *106*, 5028−5048.
(82) Sharma, S.; Dewhurst, J.; Sanna, A.; Gross, E. Bootstrap Approximation for the Exchange-Correlation Kernel of Time-Dependent Density-Functional Theory. *Physical review letters* **2011**, *107*, 186401.
(83) Wiktor, J.; Reshetnyak, I.; Ambrosio, F.; Pasquarello, A. Comprehensive Modeling of the Band Gap and Absorption Spectrum of $BiVO_4$. *Phys. Rev. Mater.* **2017**, *1*, 022401.
(84) Capelli, S. C.; Albinati, A.; Mason, S. A.; Willis, B. T. Molecular Motion in Crystalline Naphthalene: Analysis of Multi-Temperature X-ray and Neutron Diffraction Data. *J. Phys. Chem. A* **2006**, *110*, 11695−11703.
(85) Brock, C. P.; Dunitz, J. Temperature Dependence of Thermal Motion in Crystalline Anthracene. *Acta Crystallogr. B: Struct. Sci. Cryst. Eng. Mater.* **1990**, *46*, 795−806.
(86) Robertson, J. M.; Sinclair, V.; Trotter, J. The Crystal and Molecular Structure of Tetracene. *Acta Crystallogr.* **1961**, *14*, 697−704.
(87) Campbell, R.; Robertson, J. M.; Trotter, J. The Crystal and Molecular Structure of Pentacene. *Acta crystallogr* **1961**, *14*, 705−711.
(88) VandeVondele, J.; Krack, M.; Mohamed, F.; Parrinello, M.; Chassaing, T.; Hutter, J. Quickstep: Fast and Accurate Density Functional Calculations Using a Mixed Gaussian and Plane Waves Approach. *Comput. Phys. Commun.* **2005**, *167*, 103−128.
(89) Guidon, M.; Schiffmann, F.; Hutter, J.; VandeVondele, J. Ab Initio Molecular Dynamics Using Hybrid Density Functionals. *J. Chem. Phys.* **2008**, *128*, 214104.
(90) Guidon, M.; Hutter, J.; VandeVondele, J. Robust Periodic Hartree-Fock Exchange for Large-Scale Simulations Using Gaussian Basis Sets. *J. Chem. Theory Comput.* **2009**, *5*, 3010−3021.
(91) Guidon, M.; Hutter, J.; VandeVondele, J. Auxiliary Density Matrix Methods for Hartree-Fock Exchange Calculations. *J. Chem. Theory Comput.* **2010**, *6*, 2348−2364.
(92) Ishii, K.; Kinoshita, M.; Kuroda, H. Dielectric Constant Measurement on Organic Crystalline Powder. *Bull. Chem. Soc. Jpn.* **1973**, *46*, 3385−3391.
(93) Del Carro, P.; Camposeo, A.; Persano, L.; Tavazzi, S.; Campione, M.; Papagni, A.; Raimondo, L.; Silvestri, L.; Spearman, P.; Cingolani, R.; et al. Monolithic Vertical Microcavities Based on Tetracene Single Crystals. *Appl. Phys. Lett.* **2008**, *92*, 063301.
(94) Faltermeier, D.; Gompf, B.; Dressel, M.; Tripathi, A. K.; Pflaum, J. Optical Properties of Pentacene Thin Films and Single Crystals. *Phys. Rev. B* **2006**, *74*, 125416.
(95) Alvertis, A. M.; Engel, E. A. Importance of Vibrational Anharmonicity for Electron-Phonon Coupling in Molecular Crystals. *Phys. Rev. B* **2022**, *105*, L180301.
(96) Wiktor, J.; Rothlisberger, U.; Pasquarello, A. Predictive Determination of Band Gaps of Inorganic Halide Perovskites. *J. Phys. Chem. Lett.* **2017**, *8*, 5507−5512.
(97) Guo, Z.; Ambrosio, F.; Chen, W.; Gono, P.; Pasquarello, A. Alignment of Redox Levels at Semiconductor−Water Interfaces. *Chem. Mater.* **2018**, *30*, 94−111.
(98) Vydrov, O. A.; Van Voorhis, T. Nonlocal van der Waals Density Functional: The Simpler the Better. *J. Chem. Phys.* **2010**, *133*, 244103.


https://doi.org/10.1021/acs.jpclett.3c00191
J. Phys. Chem. Lett. 2023, 14, 3343−3351

(99) Sabatini, R.; Gorni, T.; de Gironcoli, S. Nonlocal van der Waals Density Functional Made Simple and Efficient. *Phys. Rev. B* **2013**, *87*, 041108.
(100) Ambrosch-Draxl, C.; Nabok, D.; Puschnig, P.; Meisenbichler, C. The Role of Polymorphism in Organic Thin Films: Oligoacenes Investigated from First Principles. *New J. Phys.* **2009**, *11*, 125010.
(101) Kronik, L.; Tkatchenko, A. Understanding Molecular Crystals with Dispersion-Inclusive Density Functional Theory: Pairwise Corrections and Beyond. *Acc. Chem. Res.* **2014**, *47*, 3208−3216.
(102) Sutton, C.; Risko, C.; Bredas, J.-L. Noncovalent Intermolecular Interactions in Organic Electronic Materials: Implications for the Molecular Packing vs Electronic Properties of Acenes. *Chem. Mater.* **2016**, *28*, 3−16.
(103) Terentjev, A. V.; Cortona, P.; Constantin, L. A.; Pitarke, J. M.; Della Sala, F.; Fabiano, E. Solid-State Testing of a van-der-Waals-Corrected Exchange-Correlation Functional Based on the Semiclassical Atom Theory. *Computation* **2018**, *6*, 7.
(104) Romani, L.; Speltini, A.; Dibenedetto, C. N.; Listorti, A.; Ambrosio, F.; Mosconi, E.; Simbula, A.; Saba, M.; Profumo, A.; Quadrelli, P.; et al. Experimental Strategy and Mechanistic View to Boost the Photocatalytic Activity of Cs3Bi2Br9 Lead-Free Perovskite Derivative by g-C3N4 Composite Engineering. *Adv. Funct. Mater.* **2021**, *31*, 2104428.
(105) Belkind, A.; Grechov, V. Energy Levels of Polyacene Crystals. *physica status solidi (a)* **1974**, *26*, 377−384.
(106) Isono, Y.; Morikawa, E.; Kotani, M. Two-Color Pulsed Photoconductivity Study of Naphthalene Single Crystal: Photoionization of Singlet Exciton. *Chemical physics letters* **1986**, *125*, 344−348.
(107) Baessler, H.; Killesreiter, H. Bandgap-Determination from Autoionization Data in Molecular Crystals. *Mol. Cryst. Liq. Cryst.* **1973**, *24*, 21−31.
(108) Riga, J.; Pireaux, J.-J.; Caudano, R.; Verbist, J. A comparative ESCA Study of the Electronic Structure of Solid Acenes: Benzene, Naphthalene, Anthracene, and Tetracene. *Phys. Scr.* **1977**, *16*, 346.
(109) Amy, F.; Chan, C.; Kahn, A. Polarization at the Gold/Pentacene Interface. *Org. Electron.* **2005**, *6*, 85−91.
(110) Zhou, Y.; Han, S.-T.; Xu, Z.-X.; Yang, X.-B.; Ng, H.-P.; Huang, L.-B.; Roy, V. Functional High-k Nanocomposite Dielectrics for Flexible Transistors and Inverters with Excellent Mechanical Properties. *J. Mater. Chem.* **2012**, *22*, 14246−14253.
(111) Brédas, J.-L.; Beljonne, D.; Coropceanu, V.; Cornil, J. Charge-Transfer and Energy-Transfer Processes in π-Conjugated Oligomers and Polymers: a Molecular Picture. *Chem. Rev.* **2004**, *104*, 4971−5004.
(112) Kera, S.; Hosoumi, S.; Sato, K.; Fukagawa, H.; Nagamatsu, S.-i.; Sakamoto, Y.; Suzuki, T.; Huang, H.; Chen, W.; Wee, A. T. S.; et al. Experimental Reorganization Energies of Pentacene and Perfluoropentacene: Effects of Perfluorination. *J. Phys. Chem. C* **2013**, *117*, 22428−22437.
(113) Coropceanu, V.; Malagoli, M.; da Silva Filho, D. A.; Gruhn, N. E.; Bill, T. G.; Brédas, J. L. Hole- and Electron-Vibrational Couplings in Oligoacene Crystals: Intramolecular Contributions. *Phys. Rev. Lett.* **2002**, *89*, 275503.
(114) Chang, B. K.; Zhou, J.-J.; Lee, N.-E.; Bernardi, M. Intermediate Polaronic Charge Transport in Organic Crystals from a Many-Body First-Principles Approach. *npj Computational Materials* **2022**, *8*, 63.
(115) McMahon, D. P.; Troisi, A. Evaluation of the External Reorganization Energy of Polyacenes. *J. Phys. Chem. Lett.* **2010**, *1*, 941−946.
(116) Freysoldt, C.; Neugebauer, J.; Van de Walle, C. G. Fully *Ab Initio* Finite-Size Corrections for Charged-Defect Supercell Calculations. *Phys. Rev. Lett.* **2009**, *102*, 016402.
(117) Komsa, H.-P.; Rantala, T. T.; Pasquarello, A. Finite-Size Supercell Correction Schemes for Charged Defect Calculations. *Phys. Rev. B* **2012**, *86*, 045112.
(118) Ambrosio, F.; Wiktor, J. Strong Hole Trapping Due to Oxygen Dimers in $BiVO_4$: Effect on the Water Oxidation Reaction. *J. Phys. Chem. Lett.* **2019**, *10*, 7113−7118.
(119) Rocco, M. L. M.; Haeming, M.; Batchelor, D. R.; Fink, R.; Schöll, A.; Umbach, E. Electronic Relaxation Effects in Condensed Polyacenes: A High-Resolution Photoemission Study. *J. Chem. Phys.* **2008**, *129*, 074702.
(120) Troisi, A. Charge Transport in High Mobility Molecular Semiconductors: Classical Models and New Theories. *Chem. Soc. Rev.* **2011**, *40*, 2347−2358.
(121) Wiktor, J.; Ambrosio, F.; Pasquarello, A. Role of Polarons in Water Splitting: The Case of $BiVO_4$. *ACS Energy Lett.* **2018**, *3*, 1693−1697.
(122) Oberhofer, H.; Reuter, K.; Blumberger, J. Charge Transport in Molecular Materials: An Assessment of Computational Methods. *Chem. Rev.* **2017**, *117*, 10319−10357.





https://doi.org/10.1021/acs.jpclett.3c00191
J. Phys. Chem. Lett. 2023, 14, 3343−3351